Eastern Denali Fault Surface Trace Map, Eastern Alaska and Yukon, Canada

By Adrian M. Bender and Peter J. Haeussler

Open-File Report 2017–1049

U.S. Department of the Interior
U.S. Geological Survey

U.S. Department of the Interior
RYAN K. ZINKE, Secretary

U.S. Geological Survey
William H. Werkheiser, Acting Director

U.S. Geological Survey, Reston, Virginia: 2017

Suggested citation:
Bender, A.M., and Haeussler, P.J., 2017, Eastern Denali Fault surface trace map, eastern Alaska and Yukon, Canada: U.S. Geological Survey Open-File Report 2017–1049, 10 p., https://doi.org/10.3133/ofr20171049.

ISSN 2331-1258 (online)

Contents

Figures

Eastern Denali Fault Surface Trace Map, Eastern Alaska and Yukon, Canada

By Adrian M. Bender and Peter J. Haeussler

Abstract

We map the 385-kilometer (km) long surface trace of the right-lateral, strike-slip Denali Fault between the Totschunda-Denali Fault intersection in Alaska, United States and the village of Haines Junction, Yukon, Canada. In Alaska, digital elevation models based on light detection and ranging and interferometric synthetic aperture radar data enabled our fault mapping at scales of 1:2,000 and 1:10,000, respectively. Lacking such resources in Yukon, we developed new structure-from-motion digital photogrammetry products from legacy aerial photos to map the fault surface trace at a scale of 1:10,000 east of the international border. The section of the fault that we map, referred to as the Eastern Denali Fault, did not rupture during the 2002 Denali Fault earthquake (moment magnitude 7.9). Seismologic, geodetic, and geomorphic evidence, along with a paleoseismic record of past ground-rupturing earthquakes, demonstrate Holocene and contemporary activity on the fault, however. This map of the Eastern Denali Fault surface trace complements other data sets by providing an openly accessible digital interpretation of the location, length, and continuity of the fault's surface trace based on the accompanying digital topography dataset. Additionally, the digitized fault trace may provide geometric constraints useful for modeling earthquake scenarios and related seismic hazard.

Introduction

The surface trace of the Denali Fault system spans more than 1,200 kilometers (km) across interior Alaska, United States and southwestern Yukon, Canada. Right-lateral, strike-slip motion along the main fault accommodates 17–30 percent of the total approximately 50 millimeters per year (mm/yr) rate of oblique collision between the Yakutat and North American Plates along the southern Alaska margin (Matmon and others, 2006; Elliott and others, 2010), with the remaining motion distributed across the collision zone in the southern Saint Elias Mountains (Pavlis and others, 2004; Doser, 2014) (fig. 1). The 2002 Denali Fault earthquake (moment magnitude 7.9) ruptured a 340-km length of the Denali Fault system in Alaska, including a branch from the main Denali Fault onto the Totschunda Fault (Eberhart-Philips and others, 2003; Haeussler and others, 2004; Schwartz and others, 2012) (fig. 1). In this report we refer to the Denali Fault east of the Totschunda-Denali Fault junction as the Eastern Denali Fault, including faults in Yukon that have been referred to as the Shakwak and Dalton Faults (Clague, 1979). Although the Eastern Denali Fault did not rupture during the 2002 earthquake, a suite of evidence demonstrates that it remains active. Such evidence includes strong historical earthquakes (surface wave magnitude 6.5 in 1944 and 6.0 in 1920; Cassidy and others, 2005), moderate background seismicity (see Doser, 2014), a paleoseismic record of at least three ground-rupturing late Holocene earthquakes (Schwartz and others, 2012), and offset landforms that indicate an average geologic slip rate of up to 8 mm/yr over the past 16–10 thousand years (Matmon and others, 2006; Seitz and others, 2008).

Thick vegetation, along with complex elongate glacial landforms, large braided rivers, and fault-parallel bedrock structure (for example, bedding), obscure the Eastern Denali Fault's surface expression. Plafker and others (1994) and Clague (1979) mapped the fault in Alaska and Yukon, respectively, providing the basis for generalized digital maps of the structure (see Koehler and others, 2012). Whereas the generalized fault trace maps provide basic information for seismic hazard models (fault location and total length), more detailed fault trace maps may reveal information about past rupture length and offset, complementing paleoseismic information and informing future field investigations (for example, see Zielke and others, 2015). The recent advent of widely available meter to centimeter resolution digital topography datasets, including digital elevation models (DEMs) based on aerial light detection and ranging (lidar) or interferometric synthetic aperture radar (IfSAR) surveys, has enabled remote mapping of active faults in unprecedented detail (for example, Meigs, 2013; Zielke and others, 2015). Additionally, the development of user-friendly photogrammetry software, such as Agisoft PhotoScan, during the past several years has allowed straightforward construction of high resolution DEMs from legacy aerial photographs, thus enhancing users' ability to visualize and map areas with aerial photograph coverage (Zielke and others, 2015 and references therein). In this study, we combine lidar, IfSAR, and photogrammetric digital topography datasets to provide a detailed digital map of the active Eastern Denali Fault surface trace (fig. 2).

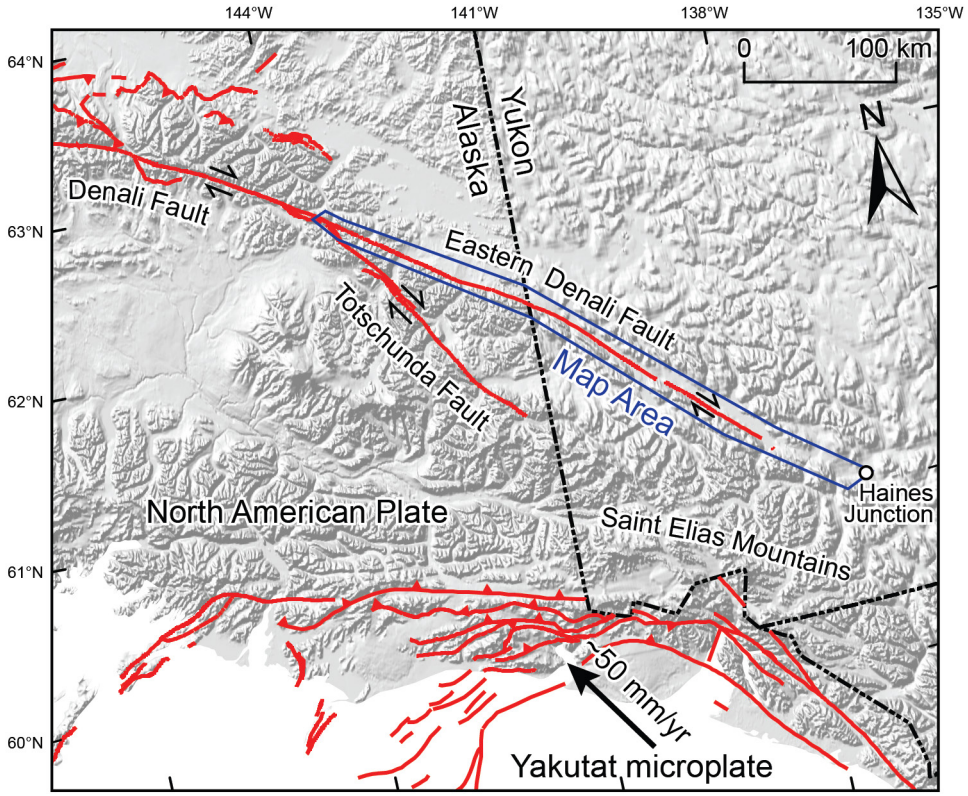

Figure 1. Map showing the tectonic setting of the Eastern Denali Fault. Active faults shown with red lines (Koehler and others, 2012), onshore area base layer is a hillshade derived from the National Elevation Dataset 2 arc-second (about 60 m/pixel) DEM, available at https://lta.cr.usgs.gov/NED, offshore area represented in white. Solid black arrow indicates the GPS-inferred velocity of the Yakutat microplate relative to the North American Plate (Elliott and others, 2010). The blue box outlines the area of the map of the Eastern Denali Fault surface trace between the Denali-Totschunda Fault junction in Alaska and Haines Junction, Yukon.

Purpose and Scope

The purposes of this report are to (1) publish digital topographic and geologic data comprising a detailed map of the surface trace of the Eastern Denali Fault and (2) to describe the methods used to create the digital data. Using a combination of lidar-, IfSAR-, and photogrammetry-based topography, we provide the first detailed (1:2,000 with lidar coverage, 1:10,000 elsewhere) interpretation of the surface trace of the nearly 385 km-long Eastern Denali Fault between the Totschunda-Denali Fault intersection in Alaska and the village of Haines Junction, Yukon. The digital topography and derivative hillshade and slope layers enable accurate location of fault-related surface features, where they exist, and provide information about cumulative vertical and horizontal surface offset across the surface trace.

Photogrammetry and Fault Trace Digitization Methods

We used Esri ArcMap (version 10.3.1) software to map the surface trace of the Eastern Denali Fault over a combination of four moderate (5 meter; m) to high (0.5 m) resolution DEMs. Hillshade and slope layers derived from the DEMs enabled visualization of fault trace features where they occur. We used 0.5 m vertical resolution DEMs and derivatives based on a 2009 EarthScope airborne lidar dataset that covers the central Denali Fault in Alaska to map the 100 km fault length between the Totschunda-Denali Fault junction and the Chisana River to the east. To map the fault trace along the 45-km length between the Chisana River and the Alaska-Yukon border, we used a 5 m/pixel DEM and derivatives based on 2010 U.S. Geological Survey IfSAR data. We are aware that TransCanada Corporation acquired a lidar dataset along the fault trace in Yukon for the purpose of understanding the related earthquake hazards, but we were unable to access or utilize the dataset in this study. In place of the TransCanada Yukon lidar dataset, we used Agisoft PhotoScan (version 1.2.3) photogrammetry software to generate dense point clouds of the fault trace between the Alaska-Yukon border and Haines Junction, Yukon, from legacy aerial photographs. We then constructed 4 m/pixel DEMs from the point clouds using Quick Terrain Modeler software (version 8.0.5.0). The supplementary table "edf_airphoto_tbl.csv" lists the aerial photographs utilized in this study. The aerial photograph orthomosaics, digital linework, and photogrammetric DEMs used in this study are publicly available online (Bender and Haeussler, 2017).

Prior to the development of the aerial photograph-based DEMs used in this study, the highest resolution topography covering the Yukon section of the Eastern Denali Fault was the Yukon 30 m/pixel DEM derived from topographic maps by Yukon Geomatics (fig. 3*A*) and available online at: www.env.gov.yk.ca/publications-maps/geomatics/data/30m_dem.php. However, since the completion of this study, two additional digital topography resources have become available: (1) a 16 m/pixel Yukon DEM, now available by searching http://geogratis.gc.ca/site/eng/download, and (2) a preliminary 2 m/pixel DEM, released by the Polar Geospatial Center at the University of Minnesota (http://pgc.umn.edu/arcticdem), that covers much of the mapped area. The current version of the 2 m/pixel ArcticDEM contains processing artifacts that distort and obscure the topographic surface over substantial parts of the Eastern Denali Fault in Yukon, whereas the DEMs we generated using PhotoScan and Quick Terrain Modeler software provide clearer, but lower resolution, coverage. Computer hardware system requirements to run ArcMap, PhotoScan, and Quick Terrain Modeler software are similar. We used a Dell Precision Tower optimized to run PhotoScan with a Dual Intel Xeon processor, Advanced Micro Devices FirePro 8-gigabyte video card, 500-gigabyte Serial-Advanced Technological Attachment hard drive, and 16 gigabytes of memory.

To generate the aerial photograph-based DEMs, we generally followed the PhotoScan tutorial workflow (available by searching www.agisoft.com), however, we modified the

workflow with the following specific steps. We acquired TIFF image scans (minimum 300 dots per inch) of legacy aerial photographs from the U.S. Geological Survey Earth Explorer web portal (earthexplorer.usgs.gov) and from Geomatics Yukon (geomaticsyukon.ca). We tended to process no more than two flight lines (up to 12 photographs) at a time in PhotoScan to maximize software efficiency. Prior to aligning the photographs in PhotoScan, we used the "smart scissors" tool to mask out fiducial marks and borders on the photographs, and constrained the alignment based on the masked photographs. Because PhotoScan relies on pixel similarity to align photographs, masking prevents misalignment of the photographs based on the recurring frame location and, unlike cropping the imported photographs outside of PhotoScan, masking does not remove useful data from the source photograph set. Before optimizing the calibration of the reconstructed camera positions, we georeferenced each set of aligned photographs. To georeference each photograph set, we identified 10–12 matching features visible in both Google Earth and in at least two photographs (for example, small closed lakes, intersecting roads, prominent bedrock features, etc.). We then used PhotoScan to create reference points on the selected features in the aerial photographs, and applied the Google Earth coordinates and elevation (provided and transcribed in GCS WGS1984 projection) of each feature to the corresponding reference point. We took coordinates in Google Earth from both Landsat and DigitalGlobe imagery covering the Yukon Eastern Denali Fault. Landsat imagery has a horizontal accuracy of about 30 m, which limited the accuracy of the coordinates in PhotoScan, and thus limited the accuracy of the derivative DEMs and orthomosaics. PhotoScan reported total reference point location errors ranging from about 7 to 80 m.

We exported the georeferenced dense point clouds from PhotoScan as LAS files, and used the adaptive triangulation gridding algorithm in Quick Terrain Modeler to construct 4 m/pixel resolution DEMs from the point clouds. The point clouds represent elevation data associated with the ground surface depicted in the source photographs, so the derivative 4 m/pixel DEMs are surface models, not terrain models. Although PhotoScan is independently capable of generating DEMs from the point clouds, we used Quick Terrain Modeler because it provides a range of options for gridding, and allows the user to progressively repair holes between points, which we did over distances as much as 12 m.

We also used PhotoScan to generate registered orthomosaics of the aerial photographs (fig. 3*C*). Visual inspection and comparison of the aerial photograph-based DEMs with both the Yukon 30-m DEM and source aerial photograph orthomosaics indicates that the aerial photograph-based DEMs are generally registered within about 30 m horizontal accuracy, similar to the accuracy associated with the coarsest Landsat imagery utilized for reference points. Locations where the aerial photograph-based DEMs appear horizontally misfit in excess of 30 m may be explained by the reported total reference point location errors that approach 80 m, or by internal inconsistencies between compared datasets.

We were unable to repair vertical discrepancies of tens of meters between the individual aerial photograph-based DEMs by registering them to other Yukon DEMs, possibly because of differences in DEM resolution. Because we lack both ground survey control and high-resolution DEMs for co-registration, and because our interpretation of fault feature location does not rely on accurate absolute elevations, we accept the vertical discrepancies and inherent limitations these place on the utility of the dataset. We consider the elevation data housed in the aerial photograph-based DEMs suitable for interpretational purposes, such as mapping, but not for quantitative analytical purposes, such as stream profile analysis. We use the orthomosaics along with hillshade and slope layers derived from the aerial photograph-based DEMs to visualize, interpret, and digitize fault-related surface features.

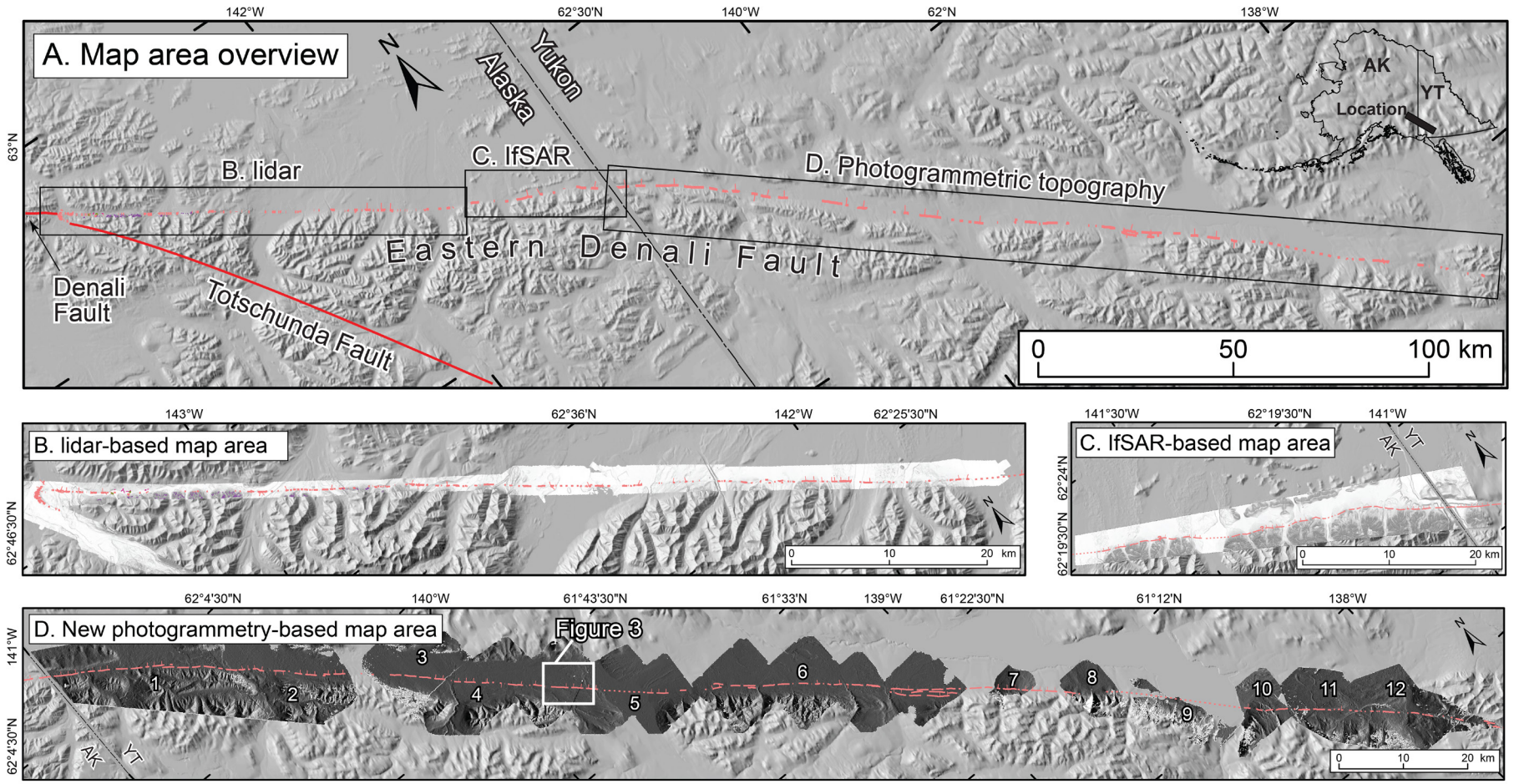

Figure 2. (*A*) Overview of the mapped area with areas of mapping based on lidar, IfSAR, and the photogrammetric topography indicated. Solid red line shows the generalized location of the Denali and Totschunda Faults; stylized light red and purple lines represent the Eastern Denali Fault surface trace mapping described in and included with this report. Abbreviations are: AK, Alaska; YT, Yukon. Detail figures show (*B*) lidar DEM-based map area, (*C*) IfSAR DEM-based map area, and (*D*) new photogrammetric topography-based map area. White numbers represent the location of the orthomosaics (1.tif–13.tif) included with this report. The base layer for figs. 2*A*–*D* is a hillshade derived from the National Elevation Dataset 2 arc-second (about 60 m/pixel) DEM, available at: https://lta.cr.usgs.gov/NED

Digitized Features

We digitized fault-related surface features including scarps, landslides, sackungen, and inferred (concealed) faults in categories determined by our confidence in the identification of each feature and the accuracy of the location of each feature given the base topography accuracy and mapping scale resolution. The shapefile attribute table contains the fields "source" and "scale" that respectively indicate the base topography used for mapping, and the associated scale of the mapping at a given location. The mapping scale of the 2009 EarthScope lidar-based DEM is 1:2,000 and the scale of mapping elsewhere is 1:10,000. Other attributes for the digitized Eastern Denali Fault surface trace features are similar to the schema used by Haeussler (2009), and all entities and attributes of the linework are described in the related metadata (edf_lines_metadata.txt).

We identified a range of geomorphic features that mark the surface trace of the Eastern Denali Fault, including linear troughs, swales, gullies, hillside benches, sub-vertical (typically east- to northeast-facing) scarps, linear sediment mounds, and linear vegetation patches prominent on the Yukon section of the fault (Clague, 1979). We mapped the Yukon length of the fault trace in close agreement with the aerial photograph- and field-based mapping of Clague (1979), and we base the location of the scarp beneath Kluane Lake on seismic reflection data shown in Figure 30.5 of Clague (1979). Although we do not significantly re-interpret Clague's (1979) mapping, the photogrammetric DEMs and orthomosaics help reveal cross-cutting relationships between the fault trace that cuts fans and gravitational deposits off of the northern Kluane Ranges front. The range front deposits overlap numerous elongate glacial landforms sub-parallel to the fault. We also distinguish the mapped fault trace from scarp-like bedrock features low on the northern Kluane Ranges front. To maintain consistency with the schema used by Haeussler (2009), we place lines at the top of sub-vertical scarps with hachures pointing down-scarp to indicate vertical displacement (indicated where the attribute "linename" includes "displacement"). In addition, landslide features occur along the Eastern Denali Fault and may have formed during past earthquakes. Similarly, sackung features present on ridges along the Eastern Denali Fault that developed either as a result of shaking during past earthquakes or from gravitational failure of the steep bedrock topography. We did not map every sackung feature archived in the different datasets owing to time constraints. Each specific feature mapped in this study is described in the shapefile attribute table field "comment." While mapping fault-related features on the underlying topographic data, we found that overlaying semi-transparent slope layers on either the hillshade or DEM provided the most effective visualization for mapping. Along the length of the Eastern Denali Fault trace in Yukon, we found that toggling between the orthomosaics and a slope layer derived from the photogrammetric DEM facilitated identification and mapping of fault-trace features.

We describe the locational accuracy of features as "accurate" or "approximate" based on our ability to locate the position of the mapped feature on the source (base) topographic data. We assign "accurate" locations to linear fault features as much as 2 mm wide at the indicated mapping scale and we assign "approximate" locations to linear fault features as much as 6 mm wide at the indicated mapping scale. Therefore, features mapped at a scale of 1:2,000 on the 2009 EarthScope lidar DEM are located "accurately" within 4 m of the mapped feature and "approximately" within 12 m. Similarly, features mapped at a scale of 1:10,000 on the 2010 U.S. Geological Survey IfSAR DEM and the photogrammetry products included with this release are located "accurately" within 20 m of the mapped feature and "approximately" within 60 m. Real world locational accuracy of the linework also varies in relation to the registration accuracy of the base topographic data that the mapping interprets.

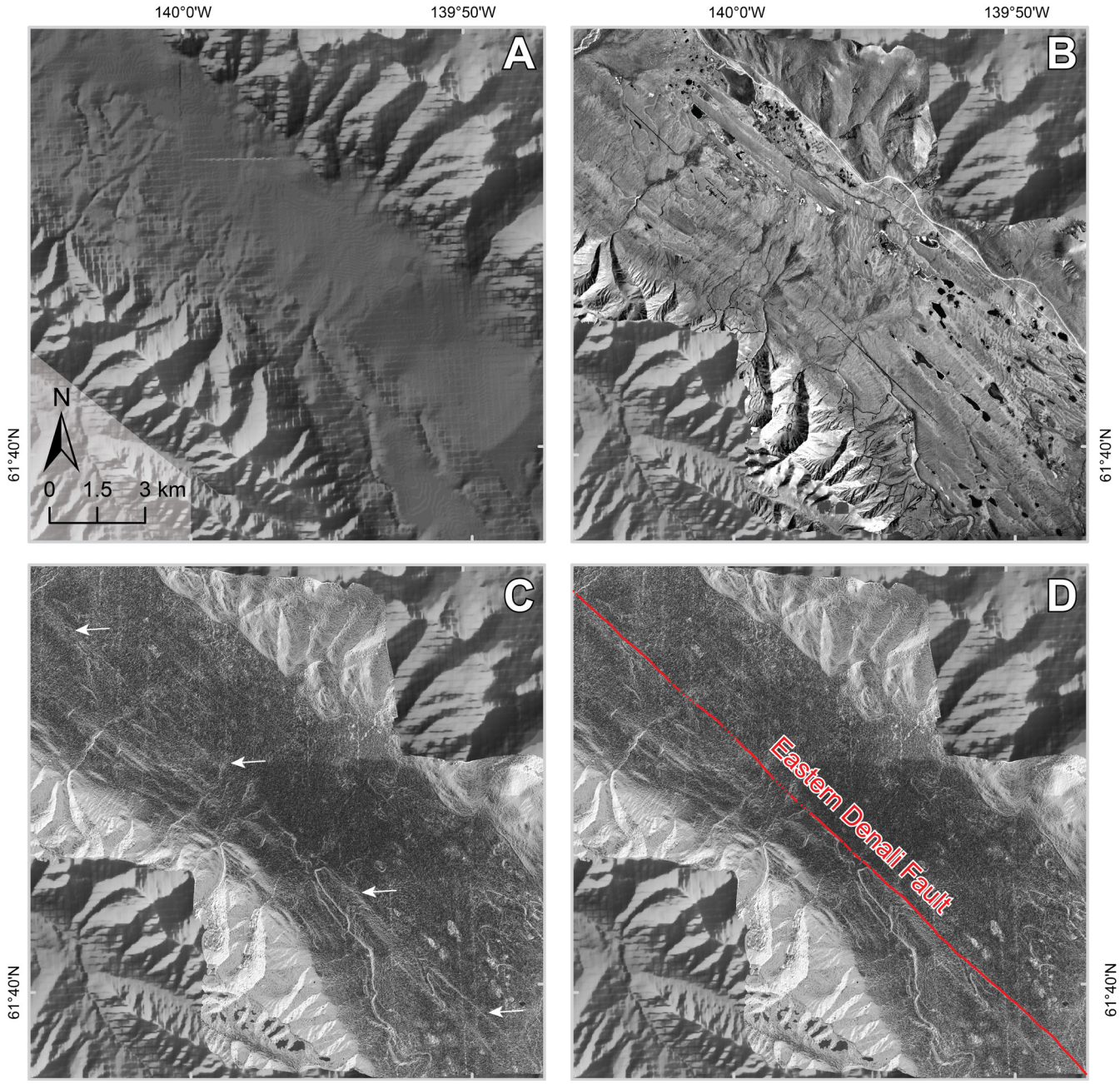

Figure 3. Close-up view of the area indicated in fig. 2*D*. (*A*) Semi-transparent hillshade derived from the Yukon 30 m DEM. At the time of this study, the 30 m DEM was the highest resolution digital topography dataset freely available for the area. (*B*) Digital scans of legacy (1979–1989) aerial photographs provided by Yukon Geomatics and orthorectified in Agisoft PhotoScan. The scans retain handwritten geomorphic interpretations from previous workers. (*C*) Semi-transparent slope over hillshade layers derived from the DEM developed in this study using Agisoft PhotoScan and legacy aerial photographs provided by Yukon Geomatics. The layers improve visualization of the surface trace of the Eastern Denali Fault, indicated by the white arrows. (*D*) The new photogrammetric topography improves visualization and facilitates improved mapping of the Eastern Denali Fault in Yukon, Canada.

Accompanying Files

The accompanying digital fault trace map, along with the DEM and orthomosaics will enable users to view, plot, and manipulate the data generated in this study using any geographic information system (GIS) software. We provide the orthomosaic files as TIFF images, labeled 1–13 in increasing order from northwest to southeast (fig. 2*D*), as well as a supplemental text file (edf_airphoto_tbl.csv) that documents the file name, year of acquisition, and digital source for each legacy aerial photograph used. We provide the aerial photograph-based DEM that covers about 90 percent of the Yukon Eastern Denali Fault as a TIFF (edf_apdem.tiff). We provide the digital fault trace map as an Esri shapefile (edf_lines.shp) with a related Esri layer file that preserves the line type styles (edf_lines.lyr). We also provide the digital fault trace map as a KML file (edf_lines.kml), and provide the attribute table as a stand-alone CSV file (edf_lines.csv). Finally, metadata associated with the orthomosaics, DEM, and digital fault trace map are included with the digital data, at https://doi.org/10.5066/F7T151WC.

Summary

We interpret lidar, photogrammetry, and IfSAR digital topography to map the surface trace of the Eastern Denali Fault between the Totschunda-Denali Fault junction in Alaska and the Village of Haines Junction in Yukon, Canada. We map 385 km of the fault surface trace at a scale of 1:2,000 on a lidar-based DEM and at a scale of 1:10,000 elsewhere, including on aerial photograph-based orthomosaics and DEMs developed in this study to visualize the length of the fault in Yukon.

Acknowledgments

We thank the National Science Foundation EarthScope program for the publicly available Denali Fault lidar dataset used in this map (available by searching www.opentopography.org). Thanks to Geomatics Yukon for providing digitized aerial photographs of the Eastern Denali Fault in Yukon. We acquired additional Yukon aerial photographs and the 30 m Yukon DEM from the USGS Earth Explorer online portal (earthexplorer.usgs.gov). The IfSAR-based DEMs used in this map are derived from radar data acquired by the U.S. Geological Survey in 2010, and are publicly available through the USGS Earth Explorer portal (earthexplorer.usgs.gov), or at ifsar.gina.alaska.edu. Thanks to C. McNeil, E. Thoms, and K. Labay for helpful guidance with the data acquisition, GIS, and photogrammetry aspects of this project. We thank E. Thoms and T. Dawson for constructive reviews of this report and related GIS data. Any use of trade, product or firm names is for descriptive purposes only and does not imply endorsement by the U.S. Government.

References Cited

Bender, A.M. and Haeussler, P.J., 2017, Eastern Denali Fault surface trace map, eastern Alaska and adjacent Canada, 1978-2008: U.S. Geological Survey data release, available at https://doi.org/10.5066/F7T151WC.

Cassidy, J.F., Rogers, G.C. and Ristau, J., 2005, Seismicity in the vicinity of the SNORCLE corridors of the northern Canadian Cordillera: Canadian Journal of Earth Sciences, v. 42, no. 6, p. 1137–1148.

Clague, J.J., 1979, The Denali fault system in southwest Yukon Territory—A geologic hazard?: Current Research, Geological Survey of Canada Paper 79-1A, v. 79, p. 169–178.

Doser, D.I., 2014, Seismicity of Southwestern Yukon, Canada, and its relation to slip transfer between the Fairweather and Denali fault systems: Tectonophysics, v. 611, p. 121–129.

Eberhart-Phillips, D., Haeussler, P.J., Freymueller, J.T., Frankel, A.D., Rubin, C.M., Craw, P., Ratchkovski, N.A., Anderson, G., Carver, G.A., Crone, A.J. and Dawson, T.E., 2003, The 2002 Denali Fault Earthquake, Alaska: A Large Magnitude, Slip-Partitioned Event: Science, v. 300, no. 5622, p. 1113–1118.

Elliott, J. L., Larsen, C. F., Freymueller, J. T., and Motyka, R. J., 2010, Tectonic block motion and glacial isostatic adjustment in southeast Alaska and adjacent Canada constrained by GPS measurements: Journal of Geophysical Research, v. 115, no. B9, 21 p.

Haeussler, P.J., 2009, Surface rupture map of the 2002 M7.9 Denali fault earthquake, Alaska; digital data: U.S. Geological Survey Data Series 422 [http://pubs.usgs.gov/ds/422/].

Haeussler, P.J., Schwartz, D.P., Dawson, T.E., Stenner, H.D., Lienkaemper, J.J., Sherrod, B., Cinti, F.R., Montone, P., Craw, P.A., Crone, A.J. and Personius, S.F., 2004, Surface rupture and slip distribution of the Denali and Totschunda faults in the 3 November 2002 M7.9 earthquake, Alaska: Bulletin of the Seismological Society of America, v. 94, no. 6B, p. S23–S52.

Koehler, R.D., Farrell, Rebecca-Ellen, Burns, P.A.C., and Combellick, R.A., 2012, Quaternary faults and folds in Alaska—A digital database *in* Koehler, R.D., Quaternary Faults and Folds: Alaska Division of Geological & Geophysical Surveys Miscellaneous Publication 141, 31 p., 1 sheet, scale 1:3,700,000, doi:10.14509/23944.

Matmon, A., Schwartz, D.P., Haeussler, P.J., Finkel, R., Lienkaemper, J.J., Stenner, H.D. and Dawson, T.E., 2006, Denali fault slip rates and Holocene–late Pleistocene kinematics of central Alaska: Geology, v. 34, no. 8, p. 645–648.

Meigs, A., 2013, Active tectonics and the LiDAR revolution: Lithosphere, v. 5, no. 2, p. 226–229.

Pavlis, T.L., Picornell, C., Serpa, L., Bruhn, R.L. and Plafker, G., 2004, Tectonic processes during oblique collision—Insights from the St. Elias orogen, northern North American Cordillera: Tectonics, v. 23, no. 3, 14 p.

Plafker, G., Gilpin, L.M., and Lahr, J.C., 1994, Neotectonic map of Alaska *in* Plafker, G., Berg, H.C., eds., The Geology of Alaska: Geological Society of America, 2 sheets, scale 1:2,500,000.

Schwartz, D.P., Haeussler, P.J., Seitz, G.G. and Dawson, T.E., 2012, Why the 2002 Denali fault rupture propagated onto the Totschunda fault—Implications for fault branching and seismic hazards: Journal of Geophysical Research, v. 117, no. B11, 25 p.

Seitz, G.J., Haeussler, P.J., Crone, A.J., Lipovsky, P., and Schwartz, D.P., 2008, Eastern Denali Fault Slip Rate and Paleoseismic History, Kluane Lake Area, Yukon Territory, Canada [abs.]: Eos (American Geophysical Union Transactions), v. 89, no. 53, supp., abstract no. T53B–1947.

Zielke, O., Klinger, Y., and Arrowsmith, J.R., 2015, Fault slip and earthquake recurrence along strike-slip faults—Contributions of high-resolution geomorphic data: Tectonophysics, v. 638, p. 43–62.

ISSN 2331-1258 (online)
https://doi.org/10.3133/ofr20171049